



OPEN Design of a class E inverter with stabilized output power using artificial neural network for applications in biomedical implants

Mehrnaz Khodadoost¹, Mohsen Hayati^{1✉} & Hamed Abbasi²

This paper presents the design, simulation, and experimental validation of a load-independent class E inverter tailored for biomedical implant applications. The proposed system addresses the challenge in the PID controller of maintaining constant output power without relying on conventional feedback circuits, which often face difficulties in accurately sensing load resistance, especially in implantable environments. To overcome this, a dual artificial neural network (ANN) architecture is introduced. The primary ANN serves as the main controller, while the secondary ANN estimates the load resistance using only the DC input voltage of the inverter and average input current. The estimated resistance is fed into the primary ANN, which regulates the system to ensure stable power delivery regardless of load variations. The inverter receives its required DC voltage from a buck converter, whose duty ratio is adjusted by the primary ANN with a mean relative error below 0.01 to maintain constant output power. Theoretical analysis, simulation, and experimental results confirm consistent performance, achieving 2 W output power at 1 MHz switching frequency. The compact and feedback-free nature of this design makes it well-suited for wireless power transfer in medical implants, wearable electronics, and portable consumer devices.

Keywords Artificial neural network, Class E inverter, PID, Control, Wireless power supply, Load independent

The class E inverter and its practical derivatives play a pivotal role as the cornerstone of wireless power transfer (WPT) systems, enabling efficient energy conversion and transmission^{1–6}. By leveraging its high-frequency switching capability and minimal power loss characteristics, it ensures optimal performance, making it indispensable for various applications such as wireless charging, biomedical devices, and industrial automation. Implantable devices like pacemakers, insulin pumps, and neural stimulators need a stable power source to function consistently and reliably^{7–9}. Robots, automated machinery in factories, HTS devices, and HTS-based wireless power transfer frequently use WPT to remove the need for wires that could hinder their movement. A stable power supply is essential for these systems to ensure uninterrupted production. In general, achieving constant power in WPT systems is essential to ensure the protection of devices, accuracy in data collection and communication, battery life preservation, and support for sensitive applications^{10–15}. This requires precise control and continuous feedback to adjust power according to the user's needs. Various works based on controllers have been proposed to control the parameters of inverters and converters. In¹⁶ introduces a full-bridge inverter with a hybrid LCLC resonant tank, controlled by the optimum asymmetrical voltage cancellation (OAVC) approach, to achieve a constant output power for plasma applications. The design and realization of a PID controlled and DC/DC converter, which offers a flexible supply voltage to achieve specific output power for a radio frequency power amplifier has been presented in¹⁷. The PID method may require a certain amount of time to eliminate input errors, and occasionally it can exhibit sluggishness. The objective of the inverter introduced in¹⁸ is to ensure its resilience against changes in load and variations in component tolerances within the output resonant filter. The concept involves implementing frequency modulation control using the hill-climbing method for regulating the output voltage in a load-independent class-E inverter. A proposal has been made in¹⁹ for the design and control of a class E inverter capable of accommodating load variations. The suggested control scheme involves dynamically adjusting the input DC voltage, switching frequency, and duty ratio in response to changes

¹Electrical Engineering Department, Faculty of Engineering, Razi University, Kermanshah 67149-67346, Iran. ²Department of Electrical Engineering, Ker.C., Islamic Azad University, Kermanshah, Iran. ✉email: mohsen_hayati@yahoo.com

in both load reactance and resistance. For application in a class-E2 dc–dc converter to manage the power flow, frequency and phase-shift control using the PI technique implemented on an FPGA has been discussed in²⁰. In²¹ a class E power amplifier using perturbation and observation (P&O) method to maximize system efficiency has been presented. The control of the power amplifier using the P&O method is associated with delays and is characterized by a slower response. In order to prevent changes in the phase difference of the output of the class E inverter resulting from the transmitter–receiver displacement, multiple relays, and capacitors have been employed in²² to correct the resonant capacitor value of the output. Consequently, the circuit dimensions have increased, and the presence of relays in the circuit introduces the possibility of magnetic disturbances. In²³, an approach to minimum input power operating point for a given output power in WPT systems has been introduced, which utilizes a maximum energy efficiency tracking (MEET) method. Notably, this method does not require any feedback from the receiver. Similar to the P&O method, the MEET method is also slow in controlling the WPT.

This paper presents the design, simulation, and fabrication of a load-independent class E inverter using two artificial neural networks (ANNs) to generate constant power independent of the load without feedback.

The structure of this article is as follows:

- Load independent class E inverter with a compensation PID controller:
In the initial phase, a class E inverter design is presented, incorporating a compensation PID controller to maintain a constant output power. Secondly, a buck converter is designed to generate the required input DC voltage for the inverter. Then, a system is developed that includes the inverter, converter, and PID controller to maintain constant output power, independent of the load. It is important to note that while a PID controller typically requires feedback from the system output, in practice, accurately measuring load resistance is often problematic.
- ANN-based solution for PID feedback replacement:
In the second section, a new methodology circuit is presented that replaces the PID controller with a primary ANN controller and substitutes the feedback system with a secondary ANN calculator. The secondary ANN takes the voltage and average input current of the inverter as inputs and solves the feedback from the output voltage and current. Its purpose is to calculate the appropriate load resistance, which is then provided as input to the primary ANN controller.

The designing of the proposed load-independent class E inverter

One of the key components influencing wireless power transfer systems in medical implants is the inverter used in the system, which is responsible for generating the required power for the proper operation of the device. Class E inverters have gained significant popularity in medical implants due to advantages such as easy construction, high power capability, and noise immunity. The main structure of a load-independent class E inverter is shown in Fig. 1a.

In the output block, as shown in Fig. 1b, the equivalent resistance between the transmitter and receiver coils in a wireless power transfer system which is established in and out of the body is represented as R_{out} . In different implants, achieving the desired power by modifying the fixed components used in the structure is a highly difficult and time-consuming task, requiring a complete redesign for each specific power requirement. To address this issue, an alternative solution must be proposed that enables the required power delivery to the load

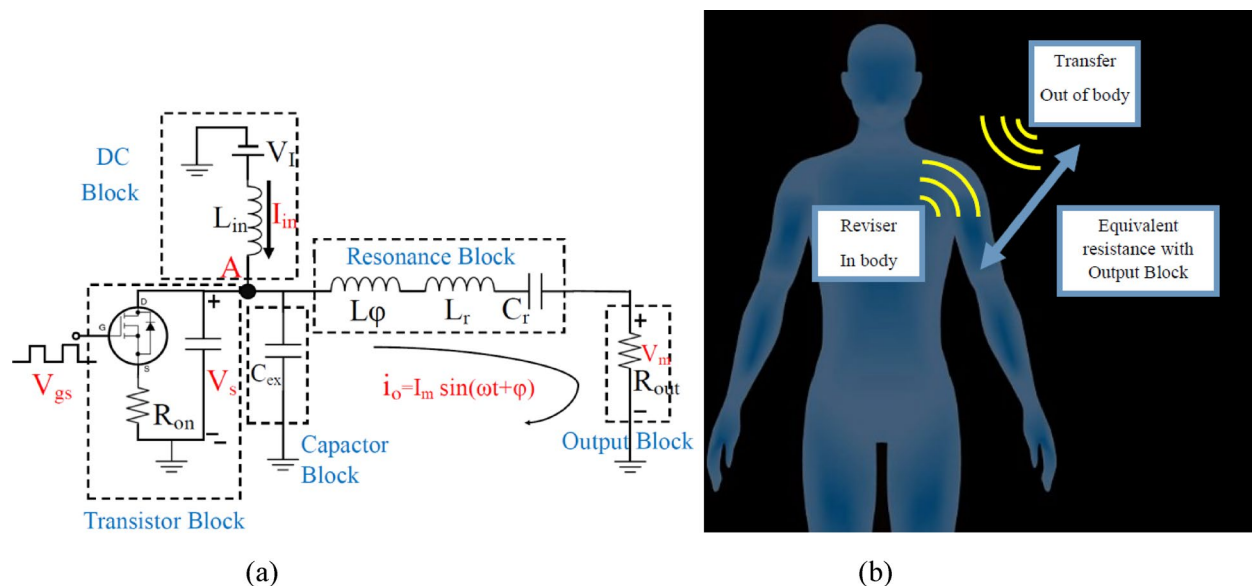


Fig. 1. (a) The proposed load-independent class E inverter. (b) Wireless power transfer system in body.

without altering the fixed components of the inverter structure. Therefore, the only adjustable element in the design as shown in Fig. 1a is the DC voltage of the inverter (V_I). The relationship between V_I , the current passing through the connected inductor in the DC block (L_{in}), and the output resistance (R_{out}) is given as follows. The transistor is off state in the range of 0 to π and on state in the range of π to 2π . Considering the output current as a pure sinusoidal waveform, the governing equations for the transistor voltage (V_s) in its off state, the capacitor current, and the current passing through the inductor L_{in} can be derived at node A based on KVL and KCL, which are expressed as:

$$dV_s(\theta)/d\theta = -\omega L_{in} d_{in}^2(\theta)/d\theta \tag{1}$$

$$i_{cex}(\theta) = \omega C_{ex} dV_s(\theta)/d\theta \tag{2}$$

$$i_{in}(\theta) = \omega C_{ex} dV_s(\theta)/d\theta + I_m \sin(\theta + \varphi) \tag{3}$$

where V_s is the switch voltage, ω represents the angular frequency calculated based on the equation $\omega = 2\pi f$, i_{in} is the current flowing through L_{in} , C_{ex} is the external capacitor and I_m is the amplitude of the output current. By combining the above-mentioned equations, a second-order differential equation based on the current passing through L_{in} is obtained, which can be solved as:

$$i_{in}(\theta) = \left(\frac{1/\omega\sqrt{L_{in}C_{ex}} \times \sin(\pi/(\omega\sqrt{L_{in}C_{ex}})) \times I_m}{(1/\omega L_{in}C_{ex} - 1) (\cos(\pi/(\omega\sqrt{L_{in}C_{ex}})) - 1)} + \frac{\pi \times V_I}{2\omega L_{in}} \right) \cos\left(\frac{1}{\omega\sqrt{L_{in}C_{ex}}}\theta\right) + \left(-\frac{1/\omega\sqrt{L_{in}C_{ex}} \times I_m}{(1/\omega L_{in}C_{ex} - 1)} \right. \\ \left. \frac{\pi (\cos \pi/(\omega\sqrt{L_{in}C_{ex}}) + 1)}{2\omega L_{in} \sin \pi/(\omega\sqrt{L_{in}C_{ex}})} \sin \frac{1}{\omega\sqrt{L_{in}C_{ex}}}\theta + \frac{1}{\omega^2 L_{in}C_{ex} - 1} I_m \sin(\theta + \varphi) \right) \tag{4}$$

In the on-state of the transistor, the inductor current L_{in} is expressed as:

$$i_{in}(\theta) = \frac{V_I}{\omega L_{in}} \times \theta - \frac{\pi V_I}{\omega L_{in}} + i_{in}(\pi) \tag{5}$$

By applying boundary conditions to determine the exact current values at the transistor's on and off transition times, specifically at $\theta=0$ and $\theta=\pi$, and also enforcing the condition of no output voltage variation based on current, which forms the basis of load-independent conditions, the inductor current L_{in} can be calculated as a function of V_I and is expressed as:

$$i_{in}(\theta) = \frac{1}{\pi} \left[\theta (1 - \cos \pi/(\omega\sqrt{L_{in}C_{ex}})) \left(\frac{1/\omega\sqrt{L_{in}C_{ex}} \times \sin \pi/(\omega\sqrt{L_{in}C_{ex}}) \times I_m}{(1/\omega L_{in}C_{ex} - 1) (\cos \pi/(\omega\sqrt{L_{in}C_{ex}}) - 1)} + \frac{\pi \times V_I}{2\omega L_{in}} \right) \right. \\ \left. - \left(-\frac{1/\omega\sqrt{L_{in}C_{ex}} \times I_m}{(1/\omega L_{in}C_{ex} - 1)} - \frac{\pi (\cos \pi/(\omega\sqrt{L_{in}C_{ex}}) + 1)}{2\omega L_{in} \sin \pi/(\omega\sqrt{L_{in}C_{ex}})} \right) \theta \sin \pi/(\omega\sqrt{L_{in}C_{ex}}) \right] \\ - 2 \left[\left(\frac{1/\omega\sqrt{L_{in}C_{ex}} \times \sin \pi/(\omega\sqrt{L_{in}C_{ex}}) \times I_m}{(1/\omega L_{in}C_{ex} - 1) (\cos \pi/(\omega\sqrt{L_{in}C_{ex}}) - 1)} + \frac{\pi \times V_I}{2\omega L_{in}} \right) \right. \\ \left. \times \left(\frac{1}{2} - \cos \pi/(\omega\sqrt{L_{in}C_{ex}}) \right) - \left(-\frac{1/\omega\sqrt{L_{in}C_{ex}} \times I_m}{(1/\omega L_{in}C_{ex} - 1)} - \frac{\pi (\cos \pi/(\omega\sqrt{L_{in}C_{ex}}) + 1)}{2\omega L_{in} \sin \pi/(\omega\sqrt{L_{in}C_{ex}})} \right) \right. \\ \left. (\sin \pi/(\omega\sqrt{L_{in}C_{ex}})) \right] \tag{6}$$

The average input current (I_{in_mean}) is influenced by two factors: the load resistance (R_{out}), which is obtained based on the change of voltage (V_m) over current (I_m), and the inverter's input voltage (V_I), as illustrated in Fig. 2. It is apparent that as the load resistance increases, the average input current of the inverter decreases. Conversely, as the inverter's input voltage increases, the input current also rises. This demonstrates that the relationship between load resistance (R_{out}), input current (I_m), and input DC voltage (V_I) is nonlinear. Therefore, to adjust the output power without changing the circuit components, the DC voltage of the load-independent inverter (V_I) needs to be changed.

Design and development of the requisite converter and PID control system

To regulate the DC input voltage of the inverter (V_I), a buck converter is required to provide a variable voltage range, allowing the output power to be adjusted to the desired level, as shown in Fig. 3. The output voltage range

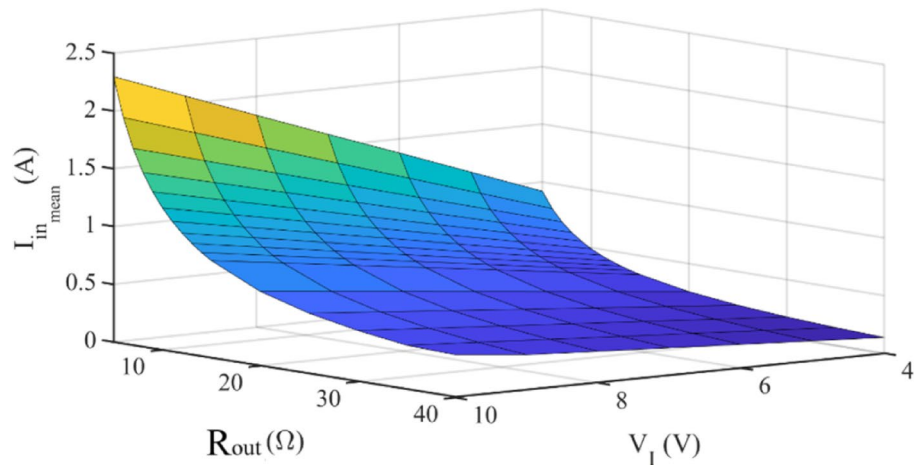


Fig. 2. The average value of the input current of the inverter versus R_{out} and V_I . Created using MATLAB version R2024a (<https://www.mathworks.com>).

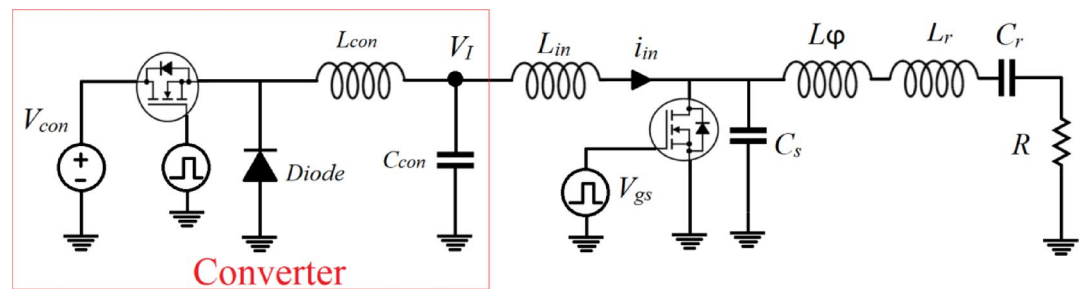


Fig. 3. The proposed converter included in the load-independent class E inverter.

of the converter can be controlled by modifying the duty ratio of the transistor used in it. The design parameters, such as the inductor value (L_{con}), can be determined using the following equation:

$$L_{con} = 1 \cdot 25 \times \frac{(1 - D)}{2 \times f} \times \frac{V_I}{I_{in}} \tag{7}$$

In Eq. (7), the value of D represents the duty ratio, f represents the frequency of the pulses applied to the transistor, V_I and I_{in} represent the output voltage and current of the converter, which are implied to the input of class E inverter. The value of L_{con} is obtained as $5 \mu\text{H}$ under worst-case conditions for an operating frequency of 1 MHz . The value of the converter circuit's capacitor (C_{con}) is obtained from the following equation:

$$C_{con} = \frac{(1 - D)}{8 \times L_{con} \times (\Delta V_I / V_I) \times f^2} \tag{8}$$

In Eq. (8), the value of ΔV_I represents the magnitude of the output voltage ripple of the converter. The value of C_{con} is determined to be $100 \mu\text{F}$.

To adjust the duty ratio of the designed converter for achieving a new set point output power, it is necessary to obtain feedback from the calculated output resistance (R_{out}) or (V_o and I_o). Additionally, a PID controller must be designed to adjust the appropriate duty ratio of the converter based on the new set power of the load, ensuring the generation of a suitable DC voltage to supply the required new power. The circuit diagram of the proposed load-independent class E inverter, along with the control duty ratio of the converter circuit designed for regulating and stabilizing the output power level in the MATLAB Simulink environment, is illustrated in Fig. 3. Presented block diagram of the intended, system with PID controller for power stabilization of an inverter is shown in Fig. 4a. The parameter values used for presented load independent class E inverter in Fig. 4b are specified in Table 1.

The parameter values presented in Table 1 were carefully selected to meet the specific operational demands and limitations of medical implant applications. Such devices commonly operate within the MHz frequency range to facilitate efficient wireless power transfer through biological tissue while minimizing the physical footprint of the implanted system. The switching frequency of 1 MHz was chosen to align with medical implant standards and to reduce the size of passive components like L_p , C_p , and C_s . The resonant elements $L_r = 55.2 \mu\text{H}$

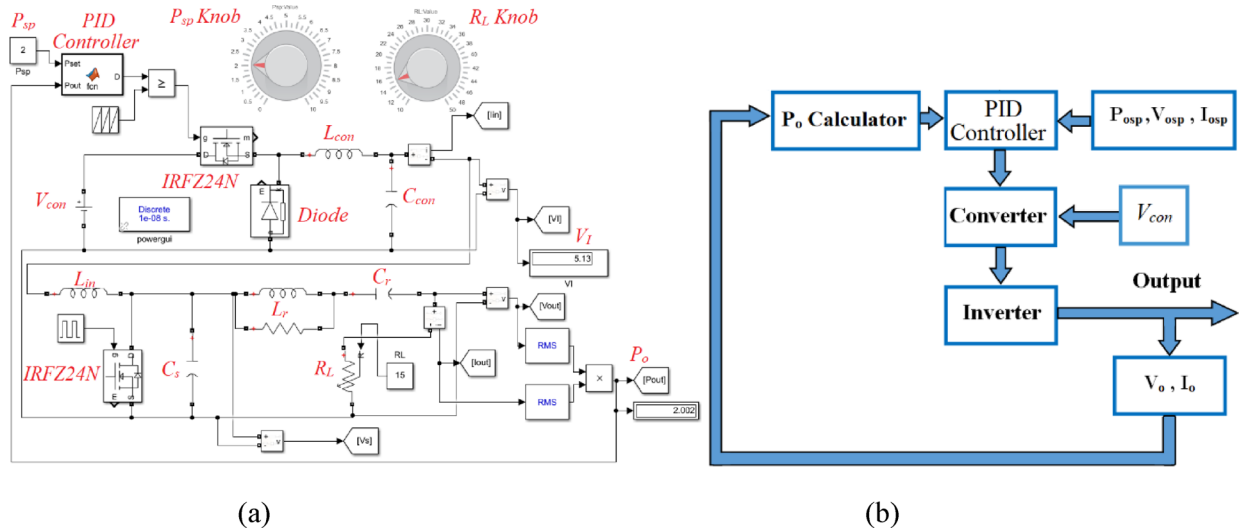


Fig. 4. (a) Presented block diagram of the intended system with PID controller for power stabilization of an inverter. (b) The proposed circuit with PID controller in MATLAB SIMULINK.

Parameters	L_{con}	C_{con}	V_{con}	L_{in}	L_r	C_r	C_s	R_L
Values	5 μ H	100 μ F	12 V	0.46 μ H	55.2 μ H	460 pF	33 nF	15 Ω

Table 1. The values of the utilized components in the proposed circuit with the PID controller.

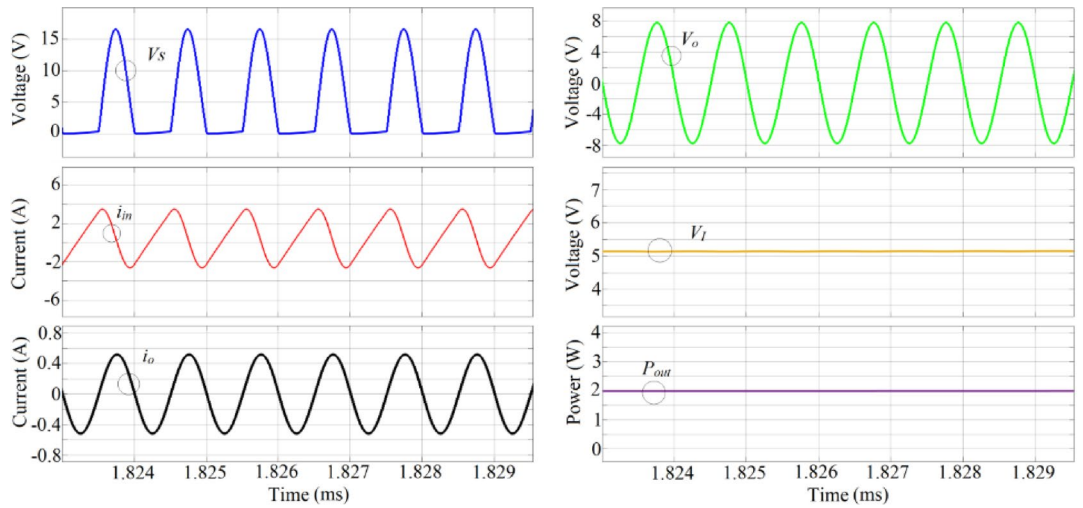


Fig. 5. Drain source voltage waveform of the transistor V_s , input current of the inverter i_{in} , output current of the inverter i_o , output voltage of the inverter V_o , input DC voltage of the inverter V_p and output power P_{out} versus time.

and $C_r = 460$ pF were specifically designed to achieve load-independent zero-voltage switching (ZVS) operation of the class E inverter at 1 MHz by the design methodologies discussed in^{24,25}. A load resistance of $R_L = 15 \Omega$ was used to emulate typical conditions found in bio-implant systems, for the converter section, components such as $C_{con} = 100 \mu\text{F}$ and $V_{con} = 12$ V were selected to ensure a stable, low-ripple DC supply to the inverter stage, crucial for the reliable performance of sensitive medical electronics. Overall, each parameter was chosen to balance efficiency, miniaturization, and safe operation within the strict biomedical constraints of implantable devices.

Figure 5 illustrates the drain-source voltage of the transistor (V_s), the inverter’s input current (i_{in}), output current (i_o), and output voltage (V_o), as well as the inverter’s input DC voltage (V_p) and output power (P_o). It can be observed that to achieve an output power of 2 W with a load resistance of 15 Ω , the converter’s output voltage

(or the inverter's input voltage) needs to be 5.13 V. Additionally, the pulse frequency for both the converter and the inverter is 1 MHz.

The voltage waveform generated by the converter, identified as the input voltage of the inverter, and the output power graph for varying load resistances of 15, 30, 45, and 15 Ω , respectively, are shown in Fig. 6. The PID controller parameters were calculated using the Ziegler–Nichols method. The proportional coefficient was set to 10, the integral coefficient to 0.002, and the derivative coefficient to 0.1. With the presented design of this PID controller, it is observed that with changes in output resistance or by changing the set point output power, the PID controller is able to efficiently stabilize the output power to a constant value of 2 W, following a few oscillations during each transition. Output power stabilization is accomplished by modifying the converter's duty cycle, which in turn adjusts the inverter's input voltage. One notable drawback of the PID controller is the relatively extended duration required to compensate for the output power. Another noteworthy factor is the significant reliance of the PID controller's coefficients on the output resistance, the converter's input DC voltage (V_{con}), and the power set point (P_{sp}). As a result, the PID controller's coefficients must be continuously updated to maintain optimal controller performance and prevent system instability under the given parameters.

Development of a load-independent class E inverter using ANN controller with secondary ANN for output feedback substitution

In practical applications such as biomedical implants, accurately measuring load resistance is often insufficient and it may lead to the addition of extra components in the structure of the wireless transmission system, such as Bluetooth or Wi-Fi modules. Also, to achieve effective feedback, a processor with a high sampling frequency analog-to-digital converter is required to precisely calculate the maximum output current and voltage, ensuring accurate load resistance determination, which practically makes this impossible. The proposed solution, as shown in Fig. 7, employs a primary ANN to replace the traditional PID controller and a secondary ANN instead of the feedback system to resolve the identified challenges. Also, in Fig. 2, it was concluded that the output resistance of the inverter can be predicted based on the DC voltage value and the current flowing through the inductor in the DC blocking section. In the presented system, the primary ANN receives the output resistance value from the secondary ANN. Considering the desired power target (P_{sp}) and the input DC voltage of the converter (V_{con}), the primary ANN calculates the necessary duty ratio to generate an appropriate input voltage for the inverter.

As illustrated, the Secondary ANN computes the necessary load resistance value for the primary ANN controller. In this instance, standard processors can effectively perform analog-to-digital conversion with sufficient accuracy. Taking into account all the aforementioned explanations, this paper employs two neural networks for Class E inverter control: one predicts the load, and the other stabilizes output power by adjusting the supply voltage through a converter. This approach uses feedback from the converter's voltage and current instead of the inverter output, simplifying the control loop and improving stability. Despite its advantages, the ANN-based control depends heavily on training data quality, assumes a fixed switching frequency, and requires retraining for new conditions. Additionally, limited real-time learning reduces adaptability in dynamic environments. The desired secondary ANN for calculating the value of the load resistance consists of a hidden layer with 5 neurons and the hyperbolic tangent sigmoid function for this layer, and the Purlin function for the output layer. This neural network has been simulated using 112 MATLAB Simulink data. 80% of these data were used for training and 20% for testing. It has a suitable mean relative error (MRE) of less than 0.01 for the test data.

Figure 8 illustrates the overall structure of the load resistance calculator ANN, along with the primary controller ANN. As evident, the initial artificial neural network obtains the load resistance value based on the V_I and I_{in_mean} and delivers it as input to the primary controller ANN. P_{sp} represents the set point power, and V_{con}

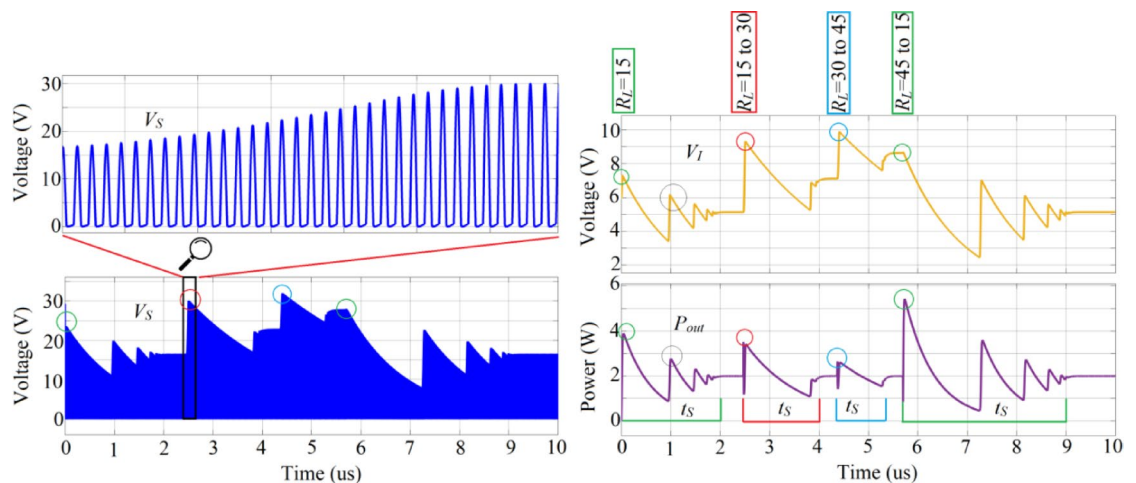


Fig. 6. V_s , V_p and P_{out} of the presented circuit with PID controller for varying load resistances of 15, 30, 45, and 15 Ω .

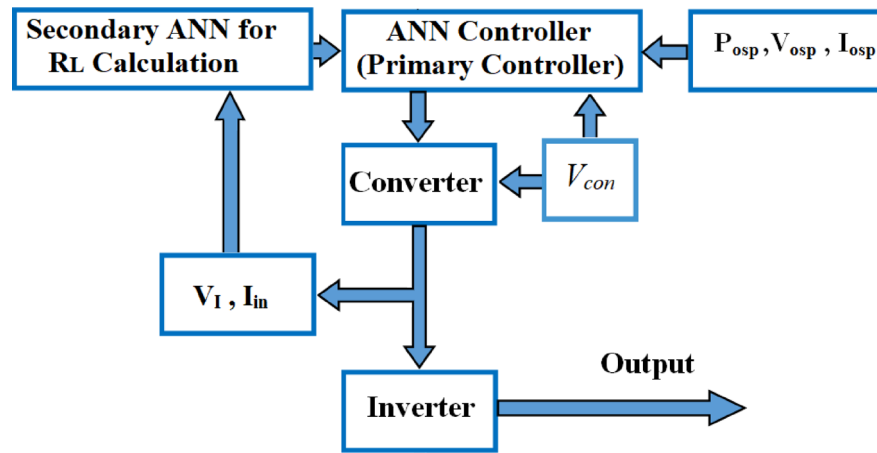


Fig. 7. Presented block diagram of the intended presented system with primary ANN controller and Secondary ANN for R_L calculation.

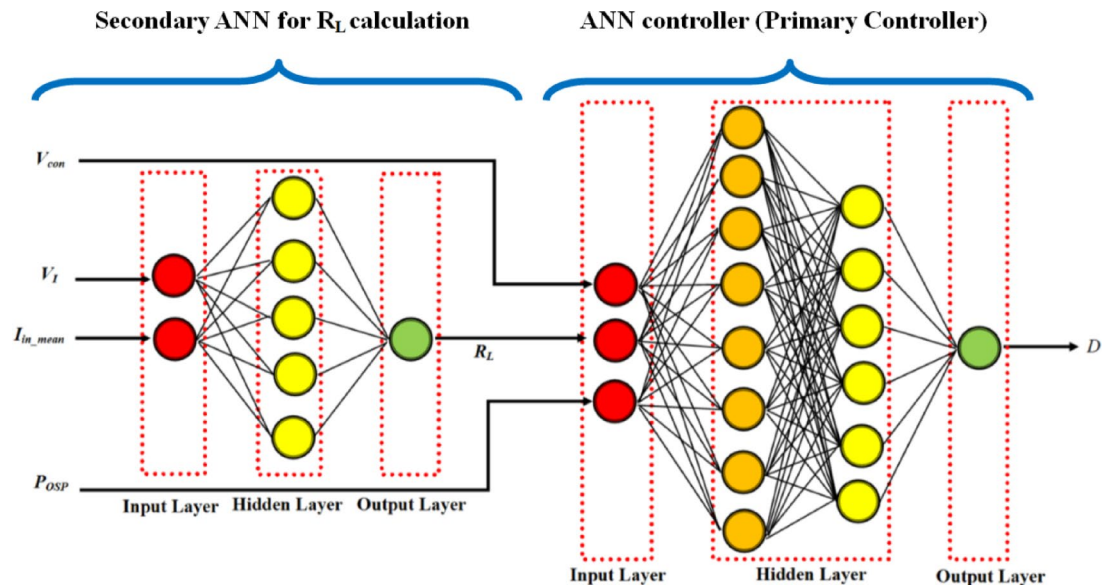


Fig. 8. The overall structure of the load resistance calculator ANN, along with the main controller ANN.

represents the applied DC voltage to the converter. D represents the Duty ratio, which is the value of the applied signal to the gate transistor of the converter. The primary ANN is considered with 8 neurons in the first layer and 6 neurons in the second layer, as shown in Fig. 8. In the first step, an artificial neural network with a single-layer architecture was designed. The activation function chosen for this layer was the tangent sigmoid, which due to its nonlinear nature has a high capacity for modeling complex relationships between data. As the number of neurons in this layer increased, the MRE consistently decreased. After 8 neurons the test error began to increase. The second hidden layer was added to the network. The activation function for the first layer remained the tangent sigmoid, while the purlin function was used for the second layer. The reason for choosing purlin is its adaptability, which provides greater flexibility and allows the network to learn more complex patterns. The results showed that as the number of neurons in the second layer increased, the MRE indicated an improvement in model performance. Specifically, the configuration with 6 neurons in the second layer resulted in the lowest error. This two-layer structure with 8 neurons in the first layer and 6 in the second was identified as the optimal configuration. The obtained MRE for the test data is 0.0063. Furthermore, the dataset used for training and testing consists of 150 data points and is obtained from the simulation results of Simulink in MATLAB.

Figure 9a represents the regression plot of the primary ANN output. As can be observed, the predicted data by the neural network aligns well with the actual data, and the regression plot forms a linear graph. Figure 9b shows the plot of actual and predicted data based on their data numbers, and similar to the regression plot, the data points exhibit a high degree of similarity to each other.

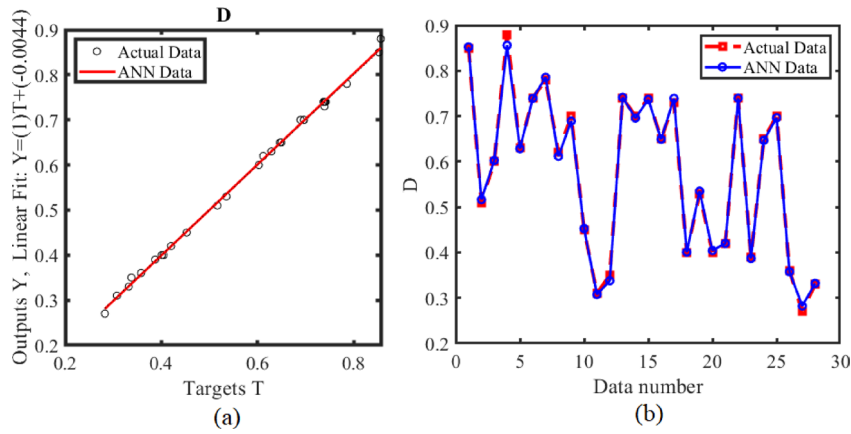


Fig. 9. (a) Regression plot of the presented ANN controller. (b) Predicted and actual output data versus data number.

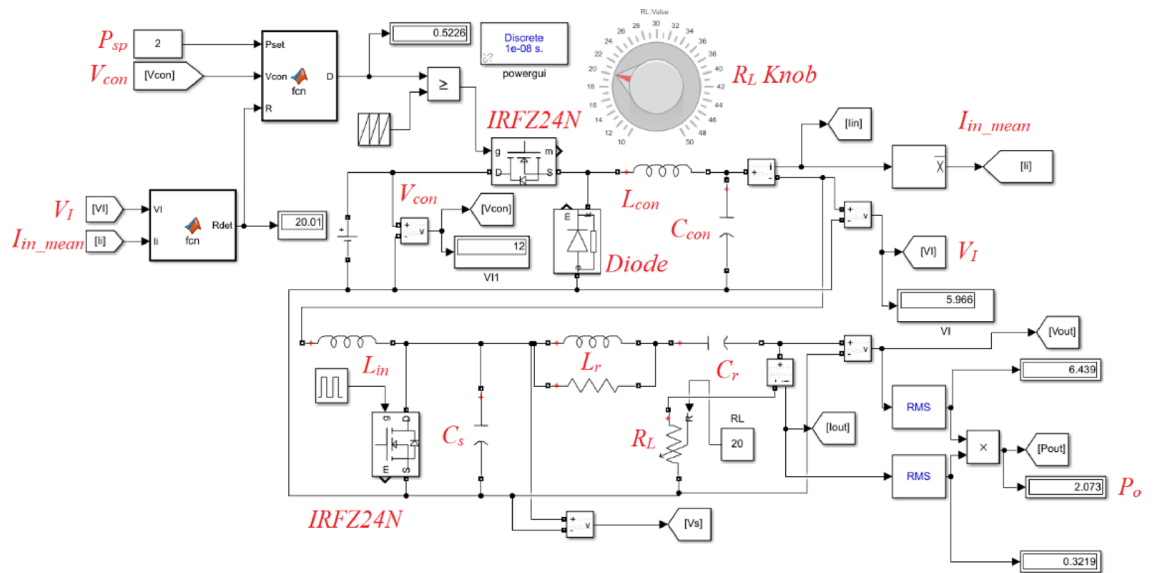


Fig. 10. The proposed circuit with ANN controller along with the load resistance calculator ANN in MATLAB SIMULINK.

Figure 10 depicts the implemented system using two implemented ANNs in MATLAB SIMULINK. As observed, the input voltage of the inverter (V_i) and the average input current of the inverter (I_{in_mean}) are sampled and fed into a neural network for detecting the load resistance value. The primary ANN, based on the load resistance, P_{sp} power, and converter voltage, determines the appropriate value of the duty ratio.

Figure 11 illustrates the voltage waveform of the inverter input, output power, and transistor voltage under varying load resistance conditions. Therefore, in this case, as previously mentioned, we can calculate the inverter load resistance without the need for output voltage and current sampling and provide it as input to the load resistance calculator ANN. In this scenario, there is no need for high-frequency sampling, and only the input DC voltage and current of the inverter are sampled.

The proposed load-independent Class E Inverter with the primary ANN controller along with the secondary ANN for R_L calculation is fabricated as shown in Fig. 12. The switching frequency plays a critical role in determining the performance of Class E inverters, influencing efficiency, output power, and stress on circuit components. While higher frequencies allow for smaller passive elements and compact designs, they also increase switching losses and electromagnetic interference, potentially lowering efficiency. Class E inverters rely on precise zero-voltage switching (ZVS) conditions, which are sensitive to frequency changes; deviations can lead to higher power dissipation and stress. Recent studies confirm that optimal frequency selection is essential for maximizing performance and efficiency. In this paper, however, frequency variation is not addressed. The control circuit, based on an Artificial Neural Network (ANN), is designed assuming a fixed switching frequency of 1 MHz, generated reliably by an STM32F103C8 microcontroller. Although the ANN-based design targets medical implants, it can be adapted to support other frequencies with proper modifications.

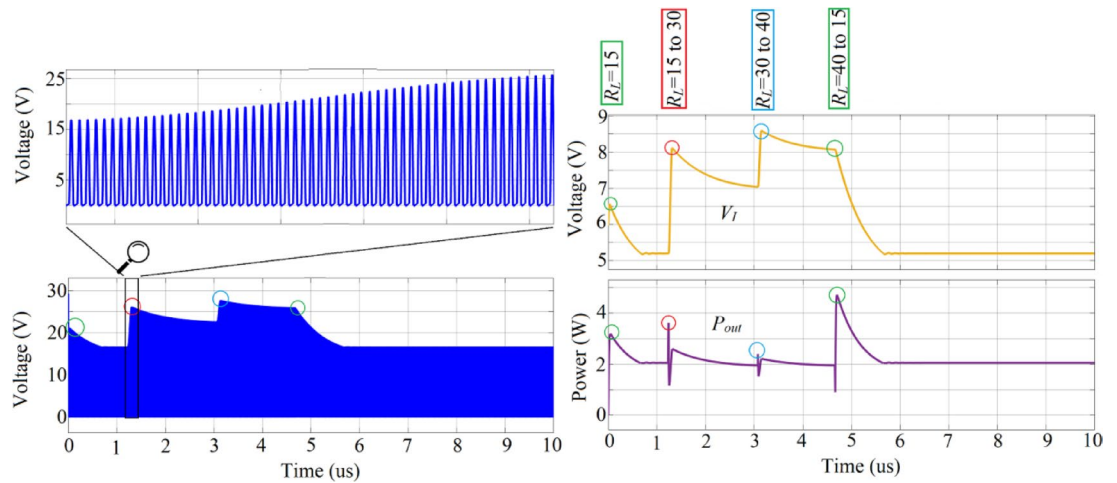


Fig. 11. The voltage waveform of the inverter input, output power, and transistor voltage under varying load resistance conditions for the proposed circuit with ANN controller along with the load resistance calculator ANN.

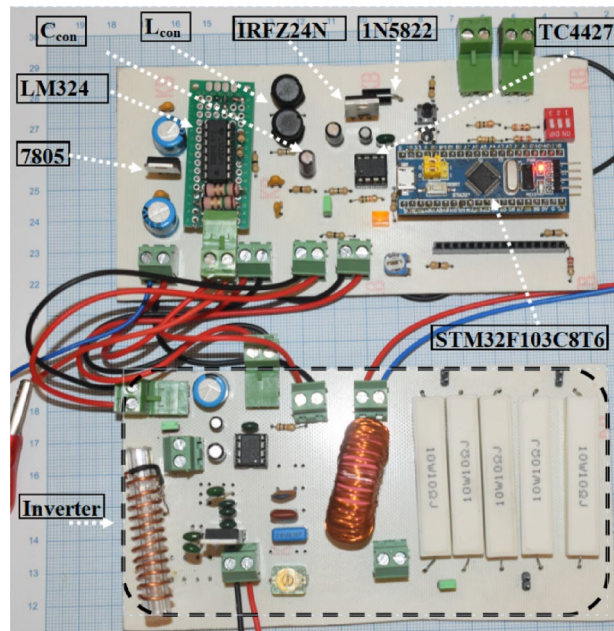


Fig. 12. The proposed class E inverter with ANN controller along with secondary ANN for R_L calculation.

The ANN architecture presented in this study is inherently adaptable and can be extended to accommodate a wide range of operating conditions. Although the current implementation is based on a fixed switching frequency and stable environmental parameters, the model can be retrained with new datasets to handle variations such as different switching frequencies, load profiles, and environmental disturbances (e.g., temperature fluctuations). This flexibility makes the proposed approach suitable for future applications in more complex and dynamic systems, where traditional feedback-based control methods may face limitations.

In the presented Class E Inverter, efficiency increases with higher load resistance and duty ratio. At lighter load resistances, conduction losses are reduced due to lower output current, and higher duty ratios lead to lower voltage stress and switching losses, resulting in improved efficiency. Figure 13 shows the variations of efficiency based on variations of duty ratio and output load resistance.

The experimental hardware presented in Fig. 12 has been designed to support different resistance values (15 Ω, 30 Ω, and 40 Ω), which were taken into account during both the design and fabrication phases. This flexibility was achieved by incorporating jumpers in the hardware layout, allowing easy selection between the three resistance values. As shown in Fig. 14, the hardware results corresponding to these three resistance values

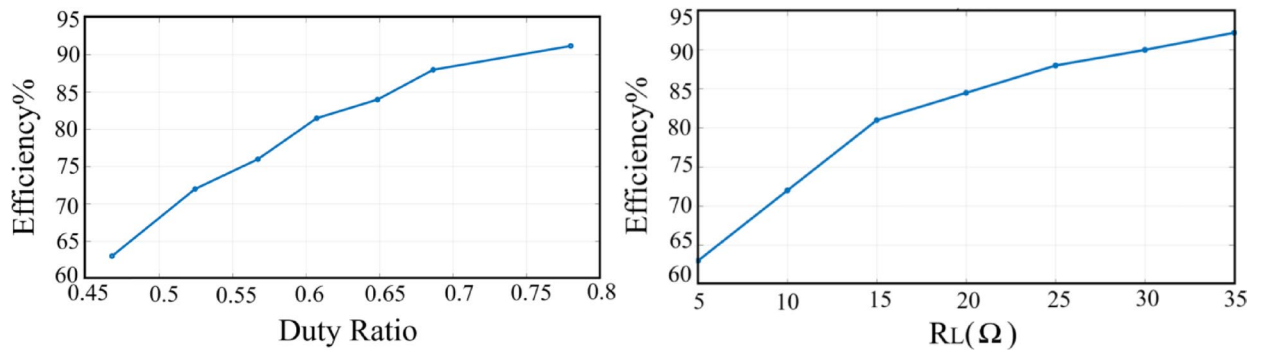


Fig. 13. Efficiency variation of the proposed class E inverter based on changes in duty ratio and output resistance (RL).

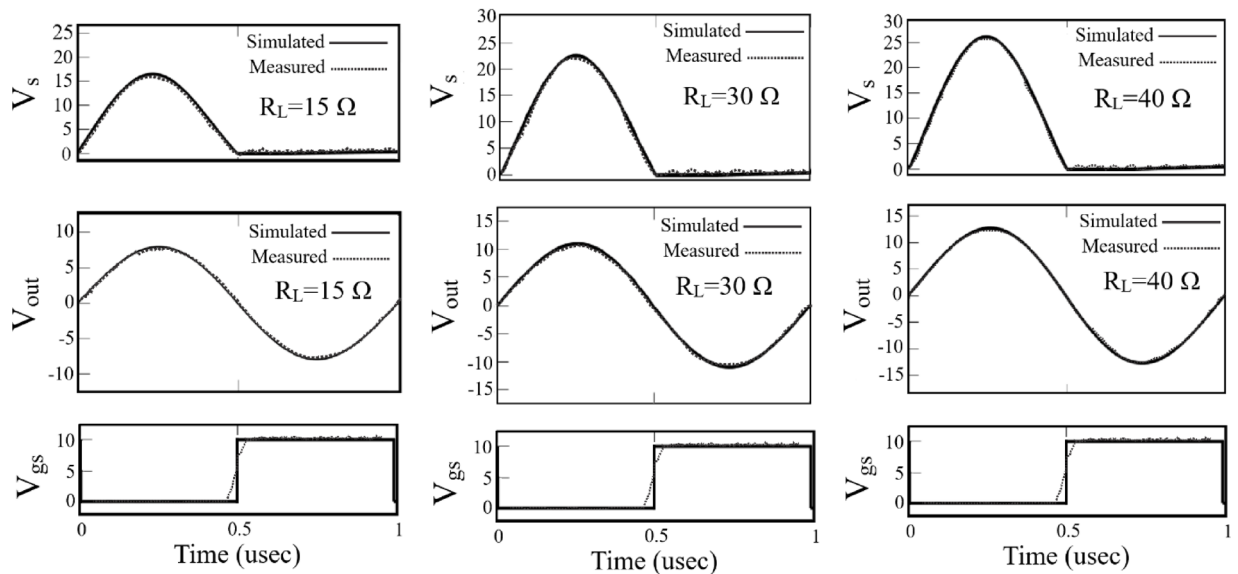


Fig. 14. The waveform of switch voltage (V_s), output Voltage (V_{out}), and voltage applied to the transistor gate in the inverter.

have been presented. These results demonstrate the practical implementation and performance of the proposed design under varying load conditions.

Figure 15 shows the results of the theory, simulation, and fabrication of the proposed system. As can be seen, the output power remains around 2 W in all three results with the change of resistive load.

Table 2 illustrates a comparison between the proposed work in this article and References. The proposed circuits in references^{12–21} have a control system. As revealed in Table 2 various methods have been presented for controlling voltage, power, and output efficiency in inverters. The duty ratio of the inverter transistor or the converter transistor providing the required DC voltage for the inverter can be adjusted, as well as the operating frequency of the inverter and the phase shift of the output voltage and current. In references^{12–18}, the PID controller has been utilized to achieve the desired set point. Although the design of the PID controller is simple, it suffers from the issue of potential system instability due to changes in plant parameters such as load resistance and input DC voltage to the inverter. Therefore, the PID controller coefficients need to be updated continuously. Additionally, during startup and system changes, the desired variables such as output power and voltage exhibit significant overshoot, which can potentially damage the transistor. As previously mentioned, the proper functioning of PID controllers relies on receiving feedback from the system's output. However, in high-frequency circuits, such as the one proposed in this study, real-time measurement of the output voltage and current not only requires high-speed operation but also necessitates the addition of extra sampling circuits at the output. This, in turn, results in additional circuitry and increased losses at the output. The Perturbation and Observation (P&O) method, which is a slow approach to reach the maximum available power at the inverter output, has been employed in^{19–21}. Although this method can also be used to reach the set point of output current or voltage, each change requires a considerable amount of correction time. In this paper, Firstly, using a PID controller, the control capability for the output power value of this inverter was designed and presented by adjusting the duty ratio of the converter circuit providing the required DC voltage input to the inverter, based on the specifications

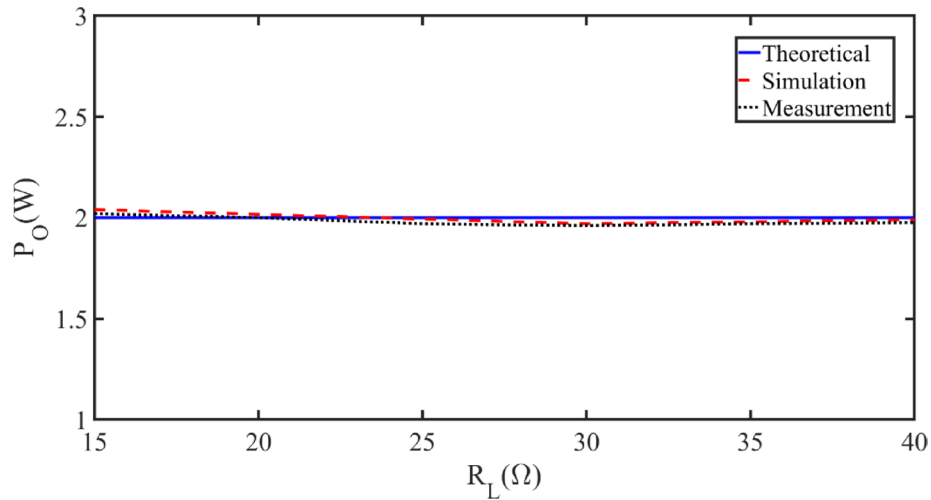


Fig. 15. P_O versus R_L variation for the presented system.

Refs.	Topology	Frequency	V_I	P_{out}	Control parameter	Controller	Method	Possible to instability
16	Class E	100 kHz	200 V	1 kW	Output power	PID	Duty ratio	Yes
17	Class E	200 kHz	5 V @ $R_L = 100 \Omega$	6 mW @ $R_{out} = 100 \Omega$	Efficiency	PID	Duty ratio	Yes
18	Class E	1 MHz	10 V @ $R_L = 20 \Omega$	5.7 W @ $R_{out} = 20 \Omega$	Output voltage	PID	Frequency	Yes
19	Class E	14 MHz	105 V @ $R_L = 50 \Omega$	200 W @ $R_{out} = 50 \Omega$	Output power	PID	Frequency, duty ratio, input DC voltage	Yes
20	Class E ²	1.5 MHz	48 V	39 W	Output power	PID	Frequency, phase shift	Yes
21	Class E	6.78 MHz	30 V @ $R_L = 22 \Omega$	10 W @ $R_{out} = 22 \Omega$	Efficiency	P&O	Converter duty ratio, input DC voltage	Yes
22	Class E	85 kHz	142.6 V	100 W @ $R_{out} = 10.14 \Omega$	Efficiency	P&O	Output matching	No
23	Class E	100 kHz	15 V @ $R_L = 50 \Omega$	4.5 W @ $R_{out} = 50 \Omega$	Efficiency	P&O	Inverter duty ratio	No
This work	Class E	1 MHz	5 V @ $R_L = 15 \Omega$	2 W @ $R_{out} = 15 \Omega$	Output power	PID	Converter duty ratio, input DC voltage	Yes
	Class E	1 MHz	5 V @ $R_L = 15 \Omega$	2 W @ $R_{out} = 15 \Omega$	Output power	ANN	Converter duty ratio, input DC voltage	No

Table 2. Comparison between the proposed inverter and references.

provided in Table 2. It was observed that the system could become unstable during changes in the plant elements and variables in the PID controller mode. Furthermore, the time required for power correction was significant. Subsequently, a novel circuit was introduced that replaces the traditional PID controller with a primary ANN controller and the feedback system with a secondary ANN calculator. The secondary ANN uses the inverter’s voltage and average input current as inputs to determine the optimal load resistance. This calculated resistance is subsequently passed to the primary ANN controller for adjusting the duty ratio of the converter circuit to supply the necessary DC voltage input to the inverter. Therefore, the desired Class E inverter was successfully presented using two ANNs, effectively addressing the issues with the PID controller, based on the specifications provided in Table 2.

Limitations and future work

While the proposed ANN-based control strategy demonstrates reliable performance under fixed operating conditions, it is important to acknowledge certain limitations. The model currently operates at a fixed switching frequency, which may limit its adaptability to systems with variable conditions. Additionally, applying the ANN to new operating scenarios requires retraining with updated datasets, which may increase implementation complexity. However, in the context of biomedical applications particularly implantable devices fixed switching frequencies are often required due to safety, electromagnetic compatibility, and regulatory standards. Therefore, this design decision remains practical and justified for the intended use case. Future work will investigate the incorporation of adaptive or online learning mechanisms to enable real-time reconfiguration of the ANN, thereby improving robustness and extending applicability to more dynamic and uncertain environments.

Conclusion

In this paper, firstly a system for selecting the desired and constant output power, comprising the designed inverter, converter, and PID controller, was presented. It was observed that while the PID controller features a simple design, it faces challenges such as system instability and significant settling time. Additionally, accurate

measurement of load resistance through feedback circuits is often difficult in practice especially in biomedical implants. As a result, the system replaces the PID controller with a primary ANN and utilizes a secondary ANN to determine the appropriate load resistance, instead of relying on feedback circuits. The secondary ANN takes the voltage and average input current of the inverter as inputs, with its primary function being to calculate the required load resistance, which is then provided as input to the primary neural network controller. The average input current to the inverter is influenced by both the load resistance and the input voltage. The desired load-independent Class E inverter delivers 2 W of output power at 1 MHz switching frequency. Theoretical, measurement, and simulation results show good agreement. This inverter is suitable for use in wireless chargers for mobile phones, smartwatches, and medical devices implanted in the body.

Data availability

The datasets generated and analyzed during the current study are available from the corresponding author on reasonable request.

Received: 28 February 2025; Accepted: 12 August 2025

Published online: 25 August 2025

References

- Raja, R., Theegala, R. & Venkataramani, B. A class-E power amplifier with high efficiency and high power-gain for wireless sensor network. *Microsyst. Technol.* **23**, 4179–4193. <https://doi.org/10.1007/s00542-016-3022-0> (2017).
- Chen, W., Chinga, R. A., Yoshida, S., Lin, J., Chen, C. & Lo, W. A 25.6 W 13.56 MHz wireless power transfer system with a 94% efficiency GaN class-E power amplifier. In *2012 IEEE/MTT-S International Microwave Symposium Digest*, 1–3 (IEEE, 2012). <https://doi.org/10.1109/mwsym.2012.6258349>.
- Wen, F., Cheng, X., Li, Q. & Ye, J. Wireless charging system using resonant inductor in class E power amplifier for electronics and sensors. *Sensors* **20**(10), 2801. <https://doi.org/10.3390/s20102801> (2020).
- Fu, M., Yin, H., Liu, M., Wang, Y. & Ma, C. A 6.78 MHz multiple-receiver wireless power transfer system with constant output voltage and optimum efficiency. *IEEE Trans. Power Electron.* **33**(6), 5330–5340. <https://doi.org/10.1109/TPEL.2017.2726349> (2017).
- Ekkaravaradome, C., Feungkeaw, S., Bilsalam, A., Jirasereamornkul, K. & Kumsuwan, Y. Analysis of a ZVDS class-DE current-driven full-bridge rectifier to compensation network capacitance design for WPT system. *AEU Int. J. Electron. Commun.* <https://doi.org/10.1109/ECTI-CON60892.2024.10594940> (2025).
- Li, T. et al. Analysis and design of voltage-source parallel resonant class E/F3 inverter. *AEU Int. J. Electron. Commun.* **187**, 155542. <https://doi.org/10.1016/j.aeue.2024.155542> (2024).
- Elliot, M., Momin, S., Fiddes, B., Farooqi, F. & Sohaib, S. A. Pacemaker and defibrillator implantation and programming in patients with deep brain stimulation. *Arrhythm. Electrophysiol. Rev.* **8**(2), 138. <https://doi.org/10.15420/aer.2018.63.2> (2019).
- Yan, B. et al. Battery-free implantable insulin micropump operating at transcutaneously radio frequency-transmittable power. *Med. Devices Sens.* **2**(5–6), e10055. <https://doi.org/10.1002/mds3.10055> (2019).
- Cagnan, H., Denison, T., McIntyre, C. & Brown, P. Emerging technologies for improved deep brain stimulation. *Nat. Biotechnol.* **37**(9), 1024–1033. <https://doi.org/10.1038/s41587-019-0244-6> (2019).
- Corti, F. et al. A comprehensive review of charging infrastructure for electric micromobility vehicles: technologies and challenges. *Energy Rep.* **12**, 545–567. <https://doi.org/10.1016/j.egy.2024.06.026> (2024).
- Lyu, R., Liu, W., Li, Q. & Chau, K. T. Overview of superconducting wireless power transfer. *Energy Rep.* **12**, 4055–4075. <https://doi.org/10.1016/j.egy.2024.09.067> (2024).
- Yan, B. et al. A review on resonant inductive coupling pad design for wireless electric vehicle charging application. *Energy Rep.* **10**, 2047–2079. <https://doi.org/10.1016/j.egy.2023.08.067> (2023).
- Zhang, Y., Huang, Z., Wang, H., Liu, C. & Mao, X. Achieving misalignment tolerance with hybrid topologies in electric vehicle wireless charging systems. *Energy Rep.* **9**, 259–265. <https://doi.org/10.1016/j.egy.2023.04.278> (2023).
- Daoud, M., Ghorbel, M. & Mnif, H. A low noise cascaded amplifier for the ultra-wide band receiver in the biosensor. *Sci. Rep.* **11**(1), 22592. <https://doi.org/10.1038/s41598-021-02122-4> (2021).
- Szuts, T. A. et al. Wireless multi-channel neural amplifier for freely moving animals. *Nat. Neurosci.* **14**(2), 263–269. <https://doi.org/10.1038/nn.2730> (2011).
- Zhao, J., Zhang, J., Din, Z. & Qian, Z. Design and implementation of high frequency power supply with constant power output for plasma applications. In *2018 IEEE Energy Conversion Congress and Exposition (ECCE)*, 6350–6355 (IEEE, 2018). <https://doi.org/10.1109/ECCE.2018.8557948>.
- Yousefzadeh, V., Wang, N., Popovic, Z. & Maksimovic, D. A digitally controlled DC/DC converter for an RF power amplifier. *IEEE Trans. Power Electron.* **21**(1), 164–172. <https://doi.org/10.1109/TPEL.2005.861156> (2006).
- Komiyama, Y., Zhu, W., Nguyen, K. & Sekiya, H. Class-E inverter with frequency modulation control. In *2021 10th International Conference on Renewable Energy Research and Application (ICRERA)*, 94–98. (IEEE, 2021). <https://doi.org/10.1109/ICRERA52334.2021.9598543>.
- Lee, J. & Ha, J. I. Design and control of high-frequency resonant inverter for wide load variation. In *2023 11th International Conference on Power Electronics and ECCE Asia (ICPE 2023-ECCE Asia)*, 909–914 (IEEE, 2023). <https://doi.org/10.23919/ICPE2023-ECCEAsia54778.2023.10213871>.
- Sawant, K., Hultman, B. & Choi, J. Frequency and phase modulation in a bidirectional class-E² converter for energy storage systems. *IEEE J. Emerg. Sel. Top. Ind. Electron.* **4**(2), 648–658. <https://doi.org/10.1109/JESTIE.2022.3231231> (2023).
- Fu, M., Yin, H., Liu, M. & Ma, C. Loading and power control for a high-efficiency class E PA-driven megahertz WPT system. *IEEE Trans. Ind. Electron.* **63**(11), 6867–6876. <https://doi.org/10.1109/TIE.2016.2582733> (2016).
- Issi, F. & Kaplan, O. Design and application of wireless power transfer using Class-E inverter based on adaptive impedance-matching network. *ISA Trans.* **126**, 415–427. <https://doi.org/10.1016/j.isatra.2021.07.050> (2022).
- Zhong, W. X. & Hui, S. Y. R. Maximum energy efficiency tracking for wireless power transfer systems. *IEEE Trans. Power Electron.* **30**(7), 4025–4034. <https://doi.org/10.1109/TPEL.2014.2351496> (2014).
- Aldaher, S., Yates, D. C. & Mitcheson, P. D. Load-independent class E/EF inverters and rectifiers for MHz-switching applications. *IEEE Trans. Power Electron.* **33**(10), 8270–8287. <https://doi.org/10.1109/TPEL.2018.2813760> (2018).
- Obinata, N., Luo, W., Wei, X. & Sekiya, H. Analysis of load-independent class-E inverter at any duty ratio. In *IECON 2019–45th Annual Conference of the IEEE Industrial Electronics Society*, 1615–1620 (IEEE, 2019). <https://doi.org/10.1109/IECON.2019.8927599>.

Author contributions

M. K. has done design, analysis, investigation, and writing original draft preparation. M. H. and H. A. have participated in supervision, validations, writing-review and editing final manuscript. All authors discussed the results and contributed to the final manuscript.

Declarations

Competing interests

The authors declare no competing interests.

Additional information

Correspondence and requests for materials should be addressed to M.H.

Reprints and permissions information is available at www.nature.com/reprints.

Publisher's note Springer Nature remains neutral with regard to jurisdictional claims in published maps and institutional affiliations.

Open Access This article is licensed under a Creative Commons Attribution-NonCommercial-NoDerivatives 4.0 International License, which permits any non-commercial use, sharing, distribution and reproduction in any medium or format, as long as you give appropriate credit to the original author(s) and the source, provide a link to the Creative Commons licence, and indicate if you modified the licensed material. You do not have permission under this licence to share adapted material derived from this article or parts of it. The images or other third party material in this article are included in the article's Creative Commons licence, unless indicated otherwise in a credit line to the material. If material is not included in the article's Creative Commons licence and your intended use is not permitted by statutory regulation or exceeds the permitted use, you will need to obtain permission directly from the copyright holder. To view a copy of this licence, visit <http://creativecommons.org/licenses/by-nc-nd/4.0/>.

© The Author(s) 2025